https://www.akustik.rwth-aachen.de
DOI: 10.18154/RWTH-2022-01536

Technical report

Documentation of the experimental environments and hardware used in the dissertation "Spatial audio reproduction for hearing aid research: System design, evaluation and application"

Florian Pausch

Institute for Hearing Technology and Acoustics, RWTH Aachen University
Kopernikusstraße 5, 52074 Aachen, Germany

Corresponding author: florian.pausch@akustik.rwth-aachen.de

Abstract: The Institute for Hearing Technology and Acoustics of RWTH Aachen University owns a number of acoustically optimised laboratories and specialised hardware, allowing the conduction of various acoustic measurements and perceptual experiments. Some of these laboratories have been improved and adapted, others were conceptualised and implemented completely from scratch, to develop the results presented in the dissertation "Spatial audio reproduction for hearing aid research: System design, evaluation and application" [1]. The key specifications of the laboratory infrastructure and hardware used are presented in this report, including compact acoustic evaluations and descriptions of the reproduction environments, spatial audio reproduction systems, and systems to measure generic and individual receiver directivities.

Keywords: virtual acoustics, spatial audio, binaural technology, experimental environments, hearing aids

1 Introduction

Motivated by the research question of how to make virtual acoustic environments accessible to HA users, a novel concept to address combined binaural sound field perception via HAs and residual hearing is introduced in Pausch [1]. While aided reproduction relies on two prototypes of research HAs, loudspeaker-based binaural reproduction is used to simulate the external sound field, requiring acoustically optimised reproduction environments.

This report contains compact descriptions of such acoustically non-ideal and ideal environments. The structures of a commercial and a custom-made hearing booth, and key specifications of a virtual reality (VR) laboratory are presented and evaluated in terms of reverberation times (RTs), clarity values and ambient noise levels (ANLs). Within the scope of the acoustic optimisation of the VR laboratory, details on the design and evaluation of the installed absorbers and their effect on RTs are presented. The first part ends with descriptions and possible application scenarios of an anechoic and a hemi-anechoic chamber.

In the second part, various hardware and software components for spatial measurements and audio reproduction with user interaction are described, including an optical motion tracking system, artificial heads, headphones with perceptually motivated equalisation (EQ) filters, and the aforementioned research HAs. The individual magnitude transfer functions of the HA microphones, measured in free-field conditions, are evaluated for a subset of spatial directions. The electroacoustic analysis extends to sound pressure level (SPL) transfer functions of the HA receivers when attached to an ear simulator using different ear pieces, and include the respective passive damping properties when blocking the ear canal during combined perception. Subsequently, three variants of loudspeaker arrays with increasing complexity, installed in the hearing booths, the VR laboratory, and the anechoic chamber, are presented and evaluated based on various acoustic measurements. The last sections of the report focus on two flexible types of measurement systems for the acquisition of generic and individual receiver directivities, ending with conclusions.

2 Reproduction environments

2.1 Commercial hearing booth

A commercially available hearing booth (A:BOX, hearing test booth, Desone Modulare Akustik, Berlin, Germany) with the dimensions 2.3 m × 2.3 m × 1.98 m (length × width × height) and a room volume of ap-

proximately 10.5 m^3 was installed at the institute [2, Fig. 4.1]. A floor carpet, fine-pore acoustic foam surface absorbers at the ceiling, six 100 mm × 50 mm × 50 mm (height × width × depth) broadband absorbers with fabric covers and a decoupled room-in-room construction enable to fulfil the specifications of audiometry standards [3–5], also rendering this experimental environment optimal for headphone-based listening experiments [2, 6, 7].

2.1.1 Room acoustics

Loudspeaker-based binaural audio reproduction is sensitive to detrimental reflections [8, 9], thus requiring reproduction environments with optimised room acoustics, typically correlating with low RTs T_{30} and high speech clarity C_{50}. To enable complementary analysis in experiments using such reproduction methods, room acoustic measurements were performed in the commercial hearing booth at 22.5 °C air temperature and a relative humidity of 37 % by reference to ISO 3382-2 [10]. Due to the extensive lining with absorbers, the sound field in the room cannot be classified as diffuse, so that the measurement results have to be interpreted correspondingly.

For the impulse response (IR) measurements, the exponential sweeps with a length of 2^{16} samples were generated at a sampling rate of 48 kHz in MATLAB™ [11] and digital-to-analog (D/A)-converted (RME Fireface UC, Audio AG, Haimhausen, Germany). Following the crossover specifications of the omnidirectional loudspeaker [12], the measurement signal was band-pass filtered and energetically band-matched using a digital loudspeaker controller (HD2, Four Audio, Herzogenrath, Germany), and conditioned for playback by a custom-made class B power amplifier. I used a 1/2″ random incidence microphone (Type 4134, Brüel & Kjær, Nærum, Denmark) with preamplifier (Type 2669, Brüel & Kjær, Nærum, Denmark) in combination with a charge amplifier (Type 2690-A, Nexus, Brüel & Kjær, Nærum, Denmark) and the same audio interface (RME Fireface UC, Audio AG, Haimhausen, Germany) to capture the sweep responses.

Although particular care was paid to optimise the two source and six receiver positions (precision level) at a height of 1.2 m above the floor, the standard requirements for the minimum distance to walls could not be met under the given space restrictions. The results for T_{30} and C_{50}, arithmetically averaged across source-receiver combinations per frequency band, are shown in Figures 1a and 1b. The mean mid-frequency RT [10] amounted to $T_{30,\mathrm{mid}} = 0.12$ s, with T_{30} values ranging from 0.12 s to 0.43 s, which entails a Schroeder frequency of about 282 Hz [13]. Clarity index values for speech ranged from 7 dB to 29 dB with an intelligibility-weighted and summed composite value C'_{50} of about 22 dB, favouring excellent speech intelligibility [14].

2.1.2 Ambient noise levels

To further investigate to which extent normative specifications as per audiometry standards [3–5] are fulfilled by this experimental environment, ANL measurements were conducted at 21.8 °C air temperature and a relative humidity of 51 % with the four loudspeakers switched on, see Section 3.5 and Table 1. I used a 1/2″ free-field low-noise microphone system (40HL, G.R.A.S. Sound & Vibration A/S, Holte, Denmark) together with a measuring amplifier (Type 2690-A, Nexus, Brüel & Kjær, Nærum, Denmark) and an audio interface (RME Madiface XT, Audio AG, Haimhausen, Germany). Placing the microphone at five random positions at a height of 1.2 m in the hearing booth, ANLs were measured for 12 s each. The measurements were evaluated for maximum time-weighted SPLs, $L_{\mathrm{Z,S,max}}$, and equivalent continuous SPLs, $L_{\mathrm{Z,eq}}$, reporting results energetically averaged across measurement cycles per frequency band. Figure 1c compares the obtained ANLs to the MPANLs for pure-tone air-conduction and bone-conduction audiometry according to ISO 8253-1 [3]. With values ranging from 0.1 dB to 35 dB, an overall ANL of 38 dB was measured. While the results per third-octave band consistently lied below the curve for MPANLs corrected for the use of normative circumaural headphones, the MPANLs for audiometries using a bone-conduction transducer were slightly exceeded in the third-octave bands with centre frequencies of 155 Hz and 4 kHz by 0.9 dB and less than 0.5 dB, respectively. Bearing measurement uncertainties in mind, the experimental environment almost completely satisfies the specifications for audiometry applications in terms of ANLs, even with the installed loudspeakers switched on.

2.2 Custom-made hearing booth

To reduce the organisational effort for supervisors and participants of listening experiments, a low cost hearing booth that can be transported to and installed at a test location closer to the participants was designed in SketchUp (Timble Inc., Sunnyvale, California, United States) and constructed by the staff of the mechanical workshop of the institute. This approach facilitates a more efficient conduction of experiments involving participants who are either young and need additional resources for transport and supervision during waiting hours, or elderly with mobility issues, preventing to travel long distances. An alternative mobile laboratory (MobiLab) with integrated hearing booth is presented by Pausch and Fels [15].

2.2.1 Design and construction

In total, the construction of the custom-made hearing booth had outer dimensions of 2.6 m × 2.6 m × 2.3 m (length × width × height) and consisted of eight wall elements. Each wall element was assembled as a frame built from 19 mm thick wood, with outer dimensions between 2.14 m × 1.24 m × 0.24 m (height × width × depth)

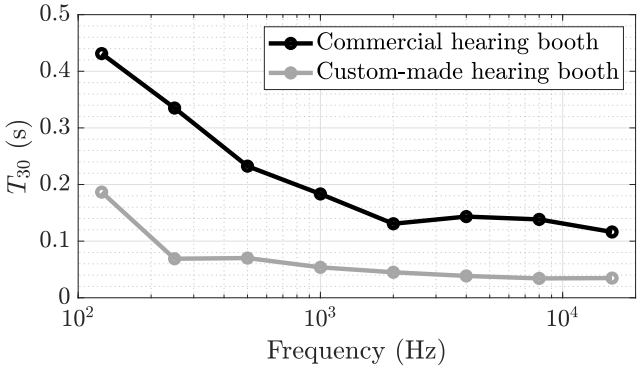

(a) Reverberation times.

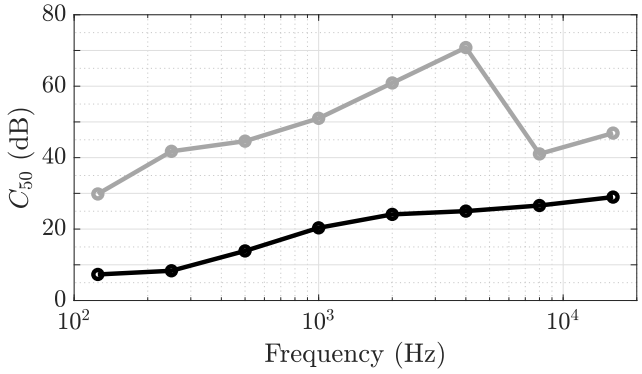

(b) Clarity index values for speech.

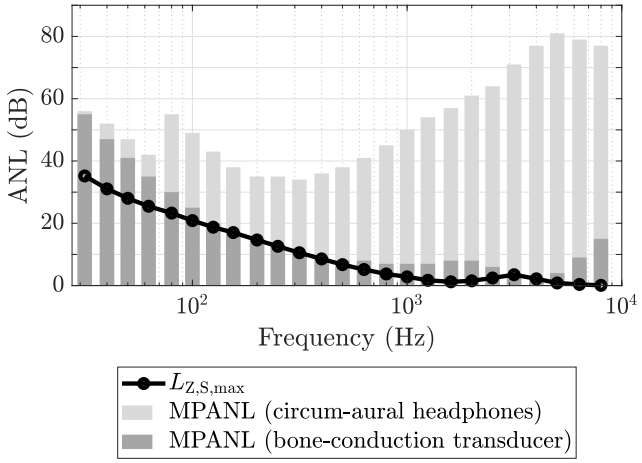

(c) Ambient noise levels.

Figure 1: (a), (b) Room acoustic parameters in the commercial and custom-made hearing booths, measured and evaluated in octave bands according to ISO 3382-2 [10], and **(c)** comparison of ANLs in the commercial hearing booth with maximum permissible ambient noise levels (MPANLs) for air-conduction and bone-conduction pure-tone audiometries according to ISO 8253-1 [3].

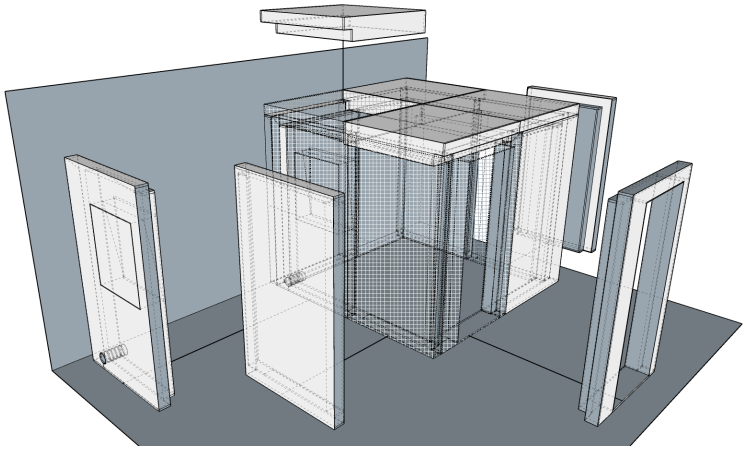

Figure 2: Construction sketch showing the individual types of elements of the custom-made hearing booth, installed in an example room.

and 2.14 m × 1.36 m × 0.24 m (height × width × depth). The four ceiling elements each measured 1.3 m × 1.3 m × 0.24 m (height × width × depth), see Figure 2. When disassembled and stacked, the elements can be transported as a package with estimated outer dimensions of 2.4 m × 2.65 m × 1.5 m (height × width × depth). I designed the wall elements in such a way that they could be inserted into one another with the other elements to create a room with internal dimensions of about 2.1 m × 2.1 m × 2 m (length × width × height), resulting in a room volume of approximately 9 m^3. On the outer shell, these elements were closed with 6 mm white plywood panels. The interspaces towards the inner space were filled with glass wool (Saint-Gobain ISOVER, Ludwigshafen, Germany) and closed with 3 mm perforated press clamping plates. On the inside, the plates

were covered with 5 mm polyether foam elements and white cloths, see Figure 10. The floor was lined with a carpet. For visual supervision, one of the wall elements holds a 0.7 m × 0.8 m (width × height) double-glazed perspex window, with a pane thickness of 5 mm each and the inner pane reinforced with glued bridges. To deflect reflections to the ceiling, the inner window was tilted upwards, and the edges of the window interspace were filled with polyether foam elements. Another wall element holds a 0.61 m × 1.98 m (width × height) door, which can be firmly closed from the outside and inside with two brackets, and is also covered with 140–150 mm thick polyether foam elements on the inside, containing a 0.28 m × 0.41 m (width × height) window. An industrial fan (Vortice S.p.A., Milan, Italy) enables to provide fresh air via a dedicated hole before the start of the experiment or during intermediate breaks. Power and signal cables permanently in use for the technical equipment inside the booth were discreetly routed via plastic pipes and white cable ducts. Additional plastic pipes, which can be filled with foam when not needed, were integrated to insert necessary cables for measurement purposes and increased practicability [16, 17].

2.2.2 Room acoustics

The same equipment as for the room acoustic measurements described in Section 2.1, except for a different microphone capsule (40AF, G.R.A.S. Sound & Vibration A/S, Holte, Denmark), was utilised. During the conduction, I measured an air temperature of 18.5 °C and a relative humidity of 30 % inside the booth. The excitation signal had a length of 2^{17} samples and was generated at a sampling rate of 44.1 kHz. The room acoustic measurements were performed and evaluated aiming at conformity with ISO 3382-2 [10] by optimising the placement of the source and the receivers, applying noise detection and compensation [18]. Meeting standard measurement precision level, the two and three source and receiver positions were measured, respectively, with two averages per combination. Subject to the spatial restrictions and similar sound field characteristics as in the commercial hearing booth, see Section 2.1, all room acoustical results described below should be interpreted equally cautious. The results for T_{30} and C_{50}, both arithmetically averaged across source-receiver combinations per frequency band, are shown in Figures 1a and 1b, respectively. The full-surface lining with absorbing material resulted in consistently lower RTs compared to the ones measured in the commercial hearing booth, amounting to values between less than 0.1 s and 0.2 s and a mean mid-frequency RT of less than 0.1 s. Consequently, the speech clarity values were also substantially higher and ranged from 30 dB to 71 dB, resulting in an excellent intelligibility-weighted and summed composite value C'_{50} of about 58 dB [14].

2.3 Virtual reality laboratory

While anechoic rooms represent highly optimised acoustic laboratories, a non-ideal reproduction environment was considered as a more commonly available option. The VR laboratory of the institute, see Figure 12b and [19, Fig. 4], with room dimensions of about 8 m × 5.3 m × 2.8 m (length × width × height) and a room volume of approximately 119 m^3, has a carpeted floor. The acoustically optimised ceiling consists of 0.6 m × 0.6 m × 0.02 m (height × width × depth) mineral wool absorber panels (Akustic SSP 2, Saint-Gobain ISOVER, Ludwigshafen, Germany) is suspended by 0.15 m and covers an area of about 26.8 m^2. One of the long side walls is equipped with six window doors, amounting to a glass area of about 11 m^2. All walls are curtained by molleton fabrics (500 g/m^2, WOOLSERGE 500, Gerriets GmbH, Umkirch, Germany). The room has two areas, the first of which is equipped with two work places (two tables and cushioned desk chairs) with computer monitors and racks holding the audio hardware. To avoid additional background noise, the computers are placed in the neighboring room and accessed remotely. The second area provides space for spatial audio reproduction, approximately spanning a floor area of about 5.57 m × 5.3 m (length × width). A 0.38 m × 0.36 m × 0.44 m (length × width × height) projector box (outer dimensions) is installed at the ceiling centre of the reproduction area, used for audio-video experiments and multi-modal demonstrations of virtual environments. For the measurements described in this thesis, one part of the curtain was placed in a way to separate the two room areas, while the three other walls in the reproduction area also remained covered with fabric.

2.3.1 Acoustic optimisation measures

To approach the requirements of ITU-R BS.1116-3 [20] in terms of RTs, I designed four plate and Helmholtz resonators [21, 22], see Figure 3, aiming to reduce the RTs below 200 Hz. Implemented as cuboid boxes with volumes of 247 ℓ and 86.5 ℓ, the plate resonators relied on a multi-layer design, consisting of 4 mm (2.6 kg/m^2 mass) and 6 mm (3.9 kg/m^2 mass) medium density fibre front plates which were inserted into custom-fit grooves. Behind the plates, air gaps of 10 mm and 80 mm, and 60 mm and 120 mm thick stone wool absorber elements (≥40 kPa s/m^2 flow resistivity, SP 120, Saint-Gobain ISOVER, Ludwigshafen, Germany), respectively, filled the remaining space. This parametrisation led to theoretical resonance frequencies and according damping coefficients of about 66 Hz and 123 Hz and 1.56 and 1.61, respectively. The Helmholtz resonators were designed as three-sided air-filled prisms with volumes of 100 ℓ and 50 ℓ. Wood panel thicknesses of 25 mm and 36 holes of 7.5 mm and 11 mm diameter with a spacing of 100 mm resulted in resonance frequencies of about 64 Hz and 124 Hz, respectively.

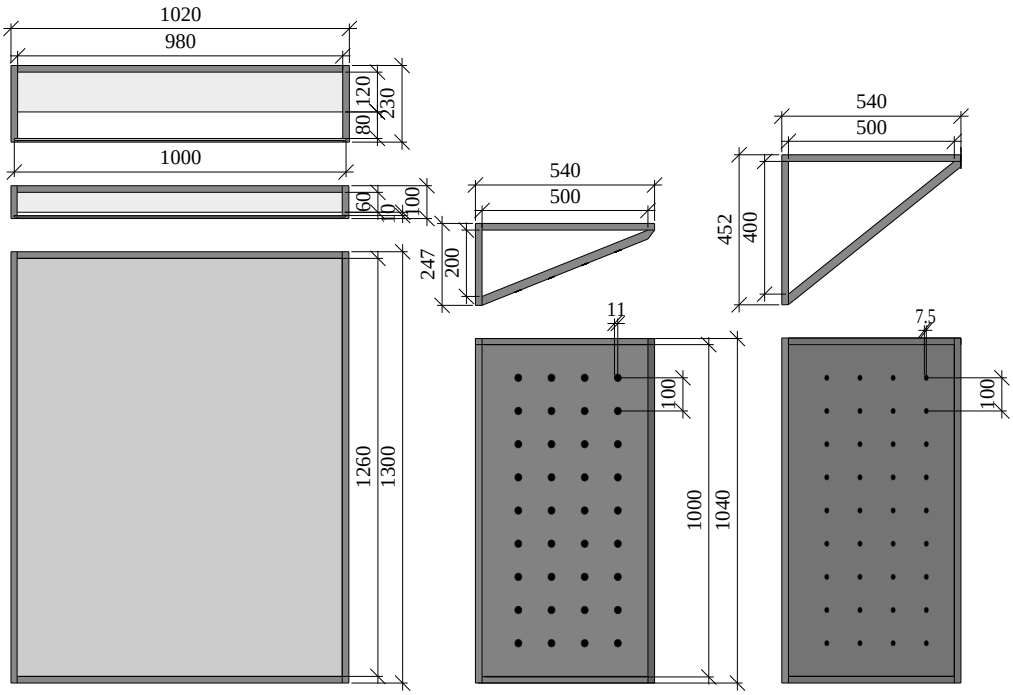

Figure 3: Top and front views of the plate resonators (left) and Helmholtz resonators (centre and right), installed in the corners of the VR laboratory. All dimensions are specified in mm.

The acoustic design verification measurements were performed in the reverberation chamber of the institute [23] according to ISO 354:2003 [24] at 19.5 °C air temperature and a relative humidity of 65 %. Pairs of the same resonator types were placed in two opposite room corners to measure their effects by comparing the resulting RTs. IRs were measured via exponential sweeps with a length of 2^{20} samples and compared to the ones obtained in the empty reverberation chamber. Figure 4 shows the determined equivalent absorption coefficients α_S and the equivalent absorption area A_T in third-octave bands with centre frequencies between 63 Hz and 5 kHz per resonance absorber, meeting the design specifications. While the two Helmholtz resonators only show distinct absorption peaks at their designed resonant frequencies, the plate resonators additionally develop a second peak at the second harmonic and thus support their respective absorber counterpart. In the VR laboratory, the two 66-Hz plate resonators were placed to fill the window cut-outs next to the room corners with the two 123-Hz plate resonators on their tops for maximum effect. Similarly, the four Helmholtz resonators were placed in the two opposite room corners.

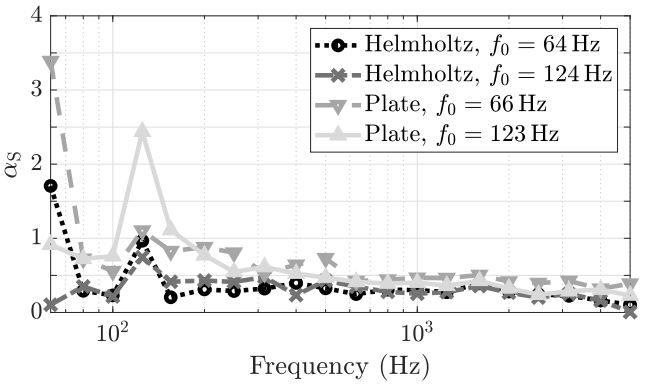

(a) Equivalent absorption coefficient.

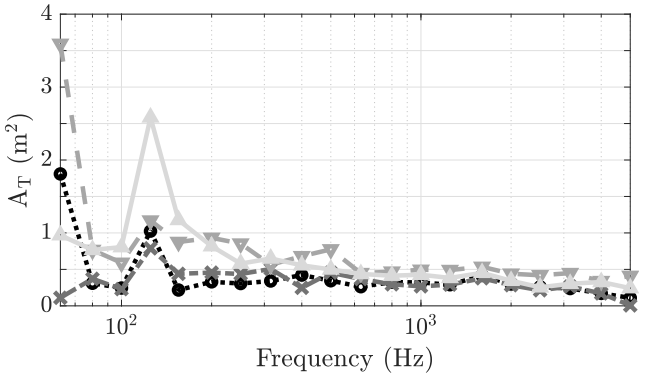

(b) Equivalent absorption area.

Figure 4: Acoustic characterisation of the resonance absorbers installed in the VR laboratory in third-octave bands per pair of the same resonant absorber type according to ISO 354:2003 [24]. The legend entries apply to both subfigures.

2.3.2 Room acoustics

For profiling purposes, room acoustic measurements were conducted as per ISO 3382-2 [10] for two source and five receiver positions (engineering measurement level) and three repetitions each, at 22.2 °C air temperature and a relative humidity of 52 %. The same equipment in the output hardware measurement chain was applied as for the room acoustic measurements in the hearing booths, except for the interface (RME Madiface USB, Audio AG, Haimhausen, Germany) and the D/A converter (A-16 MK II, Ferrofish, Linz am Rhein, Germany). The IRs were captured by a set of six microphones (KE 4, Sennheiser, Wedemark,

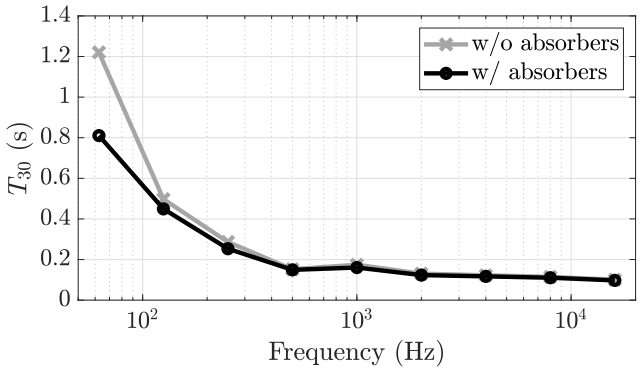

(a) Reverberation times before and after the optimisation measures.

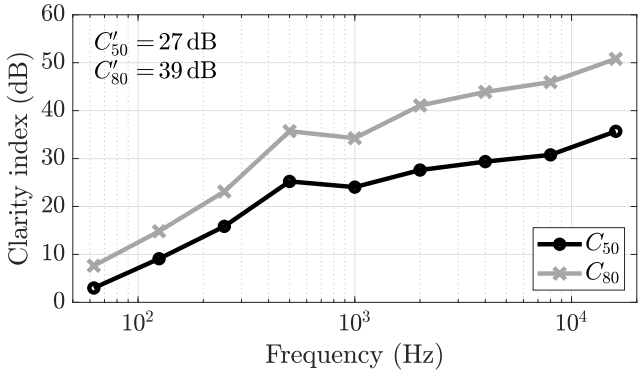

(b) Clarity indices for speech and music after the optimisation measures.

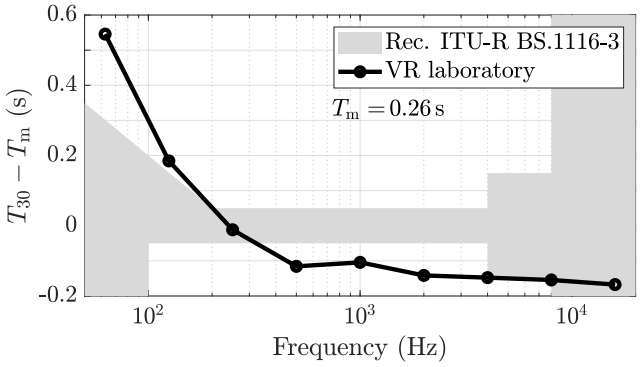

(c) Comparison of reverberation times after the optimisation measures with the tolerance range recommended by ITU-T P.57 [25].

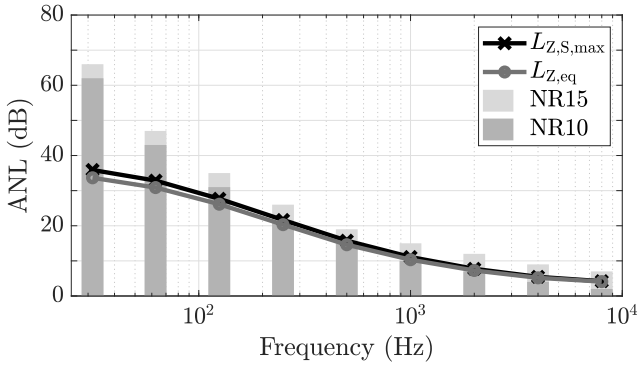

(d) Comparison of ambient noise levels with maximum permissible noise rating curves as per ISO/R 1996:1971 [26] and ITU-R BS.1116-3 [20].

Figure 5: (a), (b) Room acoustic parameters in the VR laboratory, measured and evaluated in octave bands according to ISO 3382-2 [10], with comparison to nominal **(c)** RTs and **(d)** ANLs as recommended by ITU-R BS.1116-3 [20]. The measurements were carried out in the spatial audio reproduction area, with the room walls covered with molleton fabric and a curtain separating the area from the second part of the room.

Germany) at a height of 1.2 m, pre-amplified (Ultragain Digital ADA8200, Behringer/Music Tribe Global Brands, Metro Manila, Philippines) and analog-to-digital (A/D)-converted (A-16 MKII, Ferrofish, Linz am Rhein, Germany; RME Madiface USB, Audio AG, Haimhausen, Germany).

All room acoustic parameters presented in Figure 5 were calculated per source-receiver combination [11, 27], applying noise detection and compensation [18], and subsequently arithmetically averaged across combinations per frequency band. The optimisation measures effectively decreased the RT in the lowest evaluated octave band by about 0.4 s. Although an accumulation of room modes can be calculated in this frequency range with the given room dimensions, only marginal improvements of about 0.05 s were observed for the 125-Hz band, see Figure 5a. After optimisation, a mean mid-frequency RT of $T_{30,\mathrm{mid}} = 0.15$ s (range: 0.11 s–0.81 s) was measured, resulting in a Schroeder frequency of about 72 Hz [13]. A comparison of average RTs with the tolerance region specified by ITU-R BS.1116-3 [20] using the dimensions of the empty room, see Figure 5c, showed that the low-frequency RTs are still too high and require insertion of further absorber units tuned to the room modes emerging in the corresponding frequency range. On the other hand, the octave bands with centre frequencies between 250 Hz–4 kHz seem to be over-optimised, resulting in too low RTs, which, however, can likely be corrected by partially replacing the ceiling panels with less absorbent ones. The results regarding the clarity for speech and music, C_{50} and C_{80}, ranged from 3 dB to 36 dB and 8 dB to 51 dB for speech and music, respectively. Both types of indices predict excellent clarity, given an intelligibility-weighted and summed composite value C'_{50} of about 27 dB for speech, and an averaged composite value C'_{80} of 39 dB for music [14].

2.3.3 Ambient noise levels

The same equipment and procedure was used and applied, respectively, as for the ANL measurements in the commercial hearing booth, see Section 2.1. All measurements were conducted at 22.1 °C air temperature and a relative humidity of 51 %. Figure 5d compares the

measured ANLs to the noise rating curves [26], recommended as maximum noise floor by ITU-R BS.1116-3 [20]. While $L_{Z,S,max}$ and $L_{Z,eq}$ exceeded the NR10 curve in octave bands with centre frequencies above 250 Hz and 1 kHz, respectively, there was no exceedance of the NR15 curve. With ANLs between 4 dB to 36 dB and 4 dB to 34 dB for $L_{Z,S,max}$ and $L_{Z,eq}$, respectively, overall ANLs of 38 dB and 36 dB were measured.

2.4 Hemi-anechoic chamber

The hemi-anechoic chamber of the institute was built into a cuboid exterior room with the dimensions 12.6 m×7.57 m×5.3 m (length × width × height) and a room volume of approximately 506 m^3. With almost frequency-independent average absorption coefficients smaller than 0.02 [28], the floor tiles can be considered acoustically rigid. All remaining interior room surfaces were covered with absorbent 0.8 m long wedges, which determine a lower frequency limit of about 100 Hz [29], representing a half-space free field. The acoustic provisions reduced the effective room dimensions to 11 m ×5.97 m×4.5 m (length×width×height).

This room type allows the conduction of various acoustic measurements, ranging from the characterisation of electroacoustic transducers [30], over the measurements of individual receiver characteristics [31–33], evaluation of acoustic reference scenes [28] and transfer path measurements for automotive applications [34, 35], to the determination of sound power levels of noise sources [36], which can be indirectly exploited for the calculation of sound insulation properties [15].

2.5 Anechoic chamber

The anechoic chamber of the institute was also integrated into a cuboid exterior room with the dimensions 9.2 m × 6.2 m × 5 m (length × width × height), resulting in a room volume of about 285 m^3. All room surfaces were covered with 0.7 m long glass fibre wedges, entailing a lower frequency limit of approximately 200 Hz [29]. Due to the length of the wedges, the ceiling construction and a steal wire mesh, installed about 0.2 m above the floor wedges, the effectively usable room dimensions decreased to 7.8 m × 4.9 m × 2.8 m (length × width × height). Due to the full-surface coverage with absorber elements, the room represents a free-field environment.

Anechoic chambers can be used for similar applications as listed in Section 2.4, although the floor wedges and the steal wire mesh require the installation of additional support platforms to perform some of the aforementioned measurements and perceptual investigations [37]. Compared to the hemi-anechoic counterpart, one of the main advantages of an anechoic chamber that is almost empty except for the device under test and necessary measurement equipment is that full absorbent coverage basically eliminates the need to remove unwanted reflections in measured IRs, thus allowing to preserve spectral information down to the lower frequency limit of the room. Apart from measurement applications, typically excellent shielding properties against exterior noise and stable environmental conditions further classify anechoic chambers as ideal reproduction environments for critical perceptual experiments [see, e.g. 38–40].

3 Hardware

3.1 Motion tracking systems

Electromagnetic and optical motion tracking systems can be applied to track the listener's head pose for auralisation updates in real-time [7, 41] and complementary movement analysis [2, 32].

The previous implementation of a spherical-cap loudspeaker array [42] in the anechoic chamber, see Section 2.5, was supplemented with an electromagnetic motion tracking system (PATRIOT™, Polhemus, Colchester, VT, USA) As per manufacturer specifications, this tracking system has a native frame rate of 60 Hz and a system latency of 18.5 ms. The system exhibits a static accuracy of 1.52 mm and 0.4 deg root mean square for three-dimensional sensor position and orientation data, respectively [43].

All experimental environments presented in Section 2 were equipped with optical outside-in motion tracking systems (NaturalPoint, Inc. DBA OptiTrack, Corvallis, OR, USA), featuring four (all hearing booths, the hemi-anechoic and the anechoic chambers) or six (VR laboratory) cameras (Flex 13, NaturalPoint, Inc. DBA OptiTrack, Corvallis, OR, USA). These cameras emit unobtrusive infrared light to capture a set of reflective markers mounted on the listener's head within the tracked volume. The data stream is transmitted via a tracking hub (OptiHub 2, NaturalPoint, Inc. DBA OptiTrack, Corvallis, OR, USA). Equipped with image sensors with a resolution of 1280 pixels × 1024 pixels (1.3 MP, 56° × 46° field of view), tracking objects up to 9 m away can be resolved in six degrees-of-freedom at a three-dimensional accuracy of ±0.2 mm. The system can be operated at a maximum frame rate of 120 Hz and exhibits a specified latency of 8.3 ms [44]. Prior to all experiments described in this thesis, the systems were calibrated to obtain highest possible tracking accuracy (calibration level "Exceptional") and negligible mean three-dimensional and two-dimensional reprojection and triangulation errors.

I implemented specific MATLAB™ routines [11] to communicate with MOTIVE (NaturalPoint, Inc. DBA OptiTrack, Corvallis, OR, USA) using the NatNet software development kit (NaturalPoint, Inc. DBA OptiTrack, Corvallis, OR, USA). These routines can be used, for example, for synchronised data logging, single-shot measurements, and individually translating a head-mounted rigid body to the centre of the listener's interaural axis with the help of particularly designed custom-made tracking hardware, as done for various experiments and measurements [7, 37, 41, 45] and also applied by Viveros Munoz [2] and Richter [32]. A MAT-

LAB™ interface to the real-time auralisation framework VIRTUAL ACOUSTICS [46], allowing synchronised event management, was developed by Stienen [47].

3.2 Artificial heads

Artificial heads represent a valuable tool to perform directional measurements that take into account the average anthropometric characteristics of adults or children, altering the perception of a spatialised sound source [39, 48–50].

In the scope of this thesis, I used two different adult artificial heads. The first one was designed and produced at the institute and features a simple torso but detailed ear geometry [51, 52], see [37, Fig. 1]. It is equipped with two microphones at the ear canal entrances (MK 2H, Schoeps GmbH, Karlsruhe, Germany) and microphone preamplifiers (CMC 6, Schoeps GmbH, Karlsruhe, Germany). This type of artificial head enables to measure generic HRTFs [39] or the directional transfer functions from an attached pair of research HAs [41, 53–55], see Section 3.4. It can also be used for HRTF individualisation [16, 56], or as a reference for evaluation purposes [23, 32, 57].

The second artificial head (HMS III, HEAD acoustics, Herzogenrath, Germany) is commercially available. The right ear has a detailed ear geometry and is additionally supplied with an ear simulator conforming to ITU-T P.57 [25], see Figure 13. Such artificial heads allow to account for adult ear canal characteristics to evaluate attached devices or the perception of external sound fields evaluated at artificial ear drum level [7, 41, 58].

3.3 Headphones

For experiments involving binaural reproduction via headphones, two different sets of dynamic circumaural open-back headphones (HD 600 and HD 650, Sennheiser, Wedemark, Germany) were used. Both devices cover frequency ranges exceeding the upper and lower limits of human hearing as per manufacturer specifications. Schlieper *et al.* [59] reported an occlusion index of 0.92 dB for type HD 650 headphones, indicating that the acoustic impedance is close to the open-ear acoustic impedance measured from an artficial ear (Kemar KB0066, G.R.A.S. Sound & Vibration A/S, Holte, Denmark).

For increased plausibility of headphone reproduction, the influence of the headphone transducer characteristics need to be compensated for on the basis of individual measurements. For this purpose, Masiero and Fels [60] proposed a routine to obtain perceptually robust headphone EQ filters. As an example, Figure 6 presents individual headphone transfer functions of type HD 650 headphones, measured from one individual at the blocked meatus after repositioning the headphones eight times. Additionally, the upper magnitude variance, $\mu + 2\sigma$, of the magnitude spectra and the resulting headphone EQ filter are shown. The exponential sweeps used for the measurement had a length of 2^{16} samples at a sampling rate of 44.1 kHz and were reproduced using the setup described in [37]. To avoid sharp peaks in the headphone EQ, owing to narrowband notches in the headphone transfer functions, spectral smoothing of the upper magnitude variance with a constant relative bandwidth of 1/6-th octave was applied before performing a regularised inversion between 200 Hz and 18 kHz [61]. The filter was implemented as minimum-phase filter with extrapolation of frequencies below 200 Hz towards the magnitude value measured at 200 Hz. In the last step, the filter magnitudes were normalised to the RMS of the magnitude values below 4 kHz [60], exhibiting a largely flat curve progression in this frequency range. At higher frequencies, the narrowband pinna-related notches are translated to less sharp EQ filter equivalents.

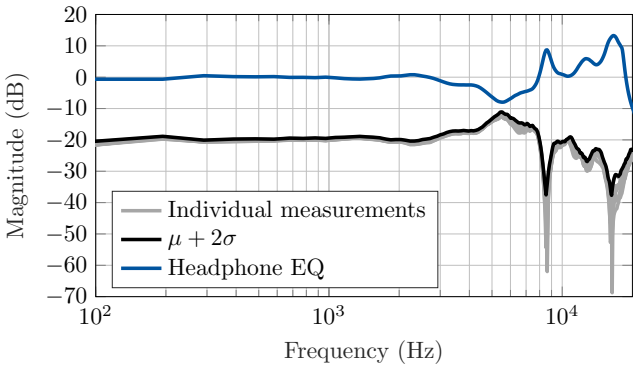

Figure 6: Example intra-individual magnitudes of headphone transfer functions with upper variance, all shifted by −20 dB for increased readability, and resulting headphone EQ filter with low-frequency extrapolation and spectral smoothing using filters with a constant relative bandwidth of 1/6-octave.

3.4 Research hearing aids

The custom-made pair of behind-the-ear receiver-in-the canal HAs (GN ReSound, Ballerup, Denmark), used for the experiments in [1], do not feature a digital signal processor but grant access to the raw microphone and HA receiver signals for transparent measurement and reproduction usage. Per device, two omnidirectional microelectro-mechanical systems microphones (Knowles, Itasca, Illinois, United States) were installed at a distance of 6.2 mm apart and approximately 1.6 mm below the housing surface, see Figure 7. Two normal-power miniature magnetic receivers (REC TUBE, NP REC, GN ReSound, Ballerup, Denmark) were used for playback, with a specified fitting range up to 90 dB hearing threshold for frequencies between 250 Hz and 1.5 kHz, and 100 dB for frequencies above, as per manufacturer specifications. For signal transmission under minimal restriction of user movements in listening experiments, the devices were connected via slim connection cables with a diameter of 1.4 mm (Hi-Pro cable, Sonion, Roskilde, Denmark).

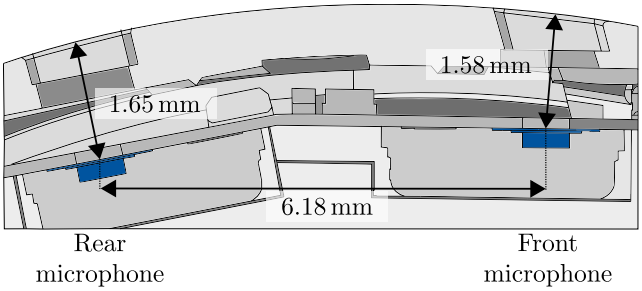

(a) Technical drawing detail with the locations of the front and rear HA microphones in blue. (Original drawing published with kind permission of GN ReSound. Drawing taken from [33], licensed under CC BY-SA 4.0, and adapted.)

(b) Photo showing the plugs for the connection cables (left side), with open dome attached to the HA receiver. (Taken from [17], licensed under CC BY 4.0, and adapted.)

Figure 7: Prototype of a behind-the-ear receiver-in-the canal HA.

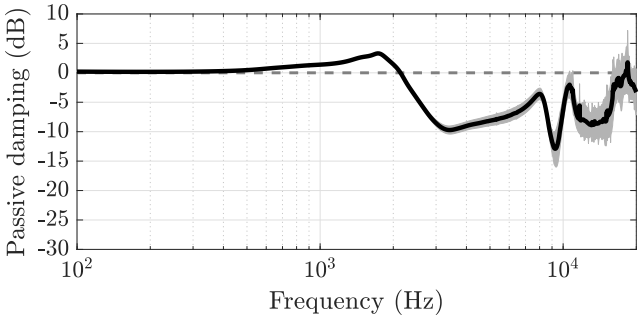

(a) Open dome.

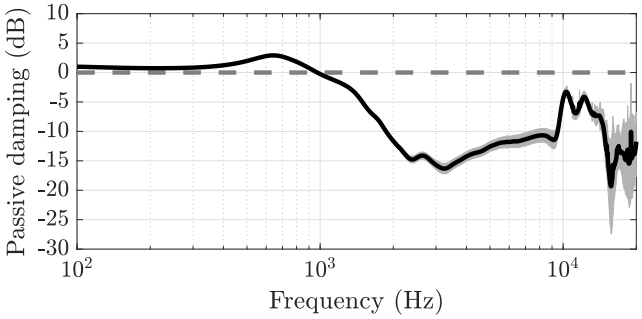

(b) Tulip dome.

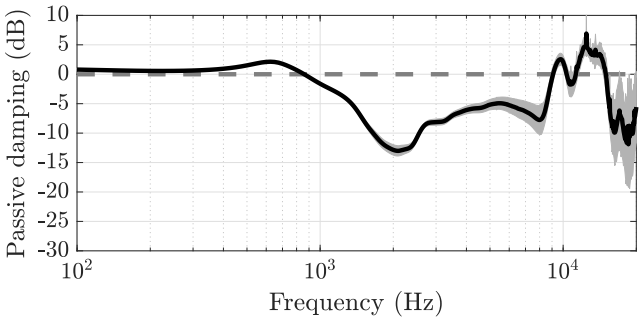

(c) Spectral difference between open and tulip domes.

Figure 8: Mean passive damping properties of the used open and tulip domes with standard deviations. The results cover directions in the horizontal plane, $\varphi \in [0°, 355°]$, and the median plane, $\theta \in [0°, 120°]$, measured in steps of 5 deg each.

3.4.1 Passive damping of open-fit ear pieces

The passive damping properties of the used silicone ear pieces need to be specified for a better understanding of the individual path contributions in combined reproduction methods with external sound field, see [1, Fig. 2.8]. For this purpose, I attached the open-dome ear piece to the HA receiver and plugged it into the right ear of the artificial head with simulator, see Section 3.2. The artificial head was mounted on the turntable as part of the measurement system in the hemi-anechoic chamber, see Section 3.8. Subsequently, the directional transfer functions between the measurement loudspeaker and the right artificial ear (Type 2610, Brüel & Kjær, Nærum, Denmark; RME Hammerfall DSP Multiface II, Audio AG, Haimhausen, Germany) with blocked ear canal (open dome, tulip dome ear pieces) were measured. The IR measurements were based on exponentially swept sines of 2^{15} samples length and covered directions in the horizontal and median planes, at azimuth and zenith angles of $\varphi \in [0°, 355°]$ and $\theta \in [0°, 120°]$, respectively, in steps of 5 deg. All measurements were performed at 22.5 °C and 42 % relative humidity. The resulting head-related IRs were time-windowed (Hann window, 2 ms fade in after 0 ms, 2 ms fade out after 10 ms) and cropped after 40 ms. Corresponding reference measurements were conducted with unblocked artificial ear canal for the same set of directions and identical post-processing. To obtain the relative spectral attenuation, the complex-valued spectra of the first and second measurements were subsequently divided.

Figure 8 displays the mean results per ear piece with standard deviations and the deviation across ear pieces. The influence of the open dome ear piece becomes gradually apparent for frequencies above about 500 Hz, resulting in a slight increase up to approximately 3 dB at 1.7 kHz caused by resonances in the blocked ear canal, before decreasing by −10 dB/octave to −10 dB. Attenuation decreases to about −4 dB, fluctuates again around the second ear canal resonance and

remains roughly constant at −8.5 dB between 11.5 kHz and 15.5 kHz with decreased damping for frequencies above. In general, the direction-dependent variation increases with increasing frequency.

In contrast, the tulip dome ear piece exhibits higher passive damping, particularly towards higher frequencies. For frequencies below 1 kHz, the decreased sound leakage allows an increased pressure chamber effect [62], which results in increased magnitude values, peaking at 2.9 dB around 680 Hz. For frequencies above 1.3 kHz, the damping becomes maximal and drops by −17 dB/octave to a maximum attenuation of −16 dB at 3.2 kHz. Similar to the open dome ear piece, the damping decreases towards the second ear canal resonance to −11 dB, strongly fluctuates due to additional resonances between 10 kHz and 15 kHz, and increases again to about −13 dB with large fluctuations.

Regarding the difference between tulip-dome and open-dome ear piece, cf. Figure 8, differences of 2 dB and −13 dB below 1 kHz and below 10 kHz, respectively, can be observed. Also at very high frequencies above about 15 kHz, the tulip dome shows much more effective damping. Collectively, the results predict more pronounced occlusion and ampclusion effects [63] and substantially higher damping of the external sound field when using the tulip dome ear piece.

3.4.2 Free-field hearing aid microphone characteristics

To selectively analyse the direction-dependent free-field HA microphone transfer functions for directions of incidence in the horizontal plane at a spatial resolution of 1 deg, the research HAs were mounted on a stand in the centre of the measurement sphere of the measurement arm, see Section 3.8. For the IR measurements, exponentially swept sines with a length of 2^{15} samples at 44.1 kHz sampling rate were generated in a frequency range between 20 Hz and 20 kHz [11]. The research HA microphone signals were amplified and A/D-converted (RME Octamic XTC, Madiface XT, Audio AG, Haimhausen, Germany). For the conditioning of the loudspeaker signal, I used a custom-made measurement front-end and power amplifier (ITADDA16, Institute of Technical Acoustics, RWTH Aachen, Germany) [64, Fig. 1], the output signal of which was fed to the measurement loudspeaker. To remove the influence of the measurement loudspeaker, reference IR measurements were performed using a free-field microphone (40 AF, G.R.A.S. Sound & Vibration A/S, Holte, Denmark) with microphone preamplifier (Type 2669, Brüel & Kjær, Nærum, Denmark) and conditioning amplifier (Type 2690-A, Nexus, Brüel & Kjær, Nærum, Denmark). Before conducting the spectral division with regularisation in a frequency range of 100 Hz to 20 kHz [65], all IRs were windowed in time domain (one-sided Hann windows, 1 ms fade-in after 0 ms, 1 ms fade-out after 9 ms). The resulting median free-field transfer functions with interquartile ranges of the research HA microphones, grouped in front and rear microphone pairs, are shown in Figure 9a. While the front microphone pair exhibit a very similar frequency response with an approximately constant offset of 1.5 dB below about 8 kHz, the rear microphone pair show a more consistent behaviour up to 6 kHz before stronger deviations occured for frequencies above, including more pronounced direction-dependent variations per device.

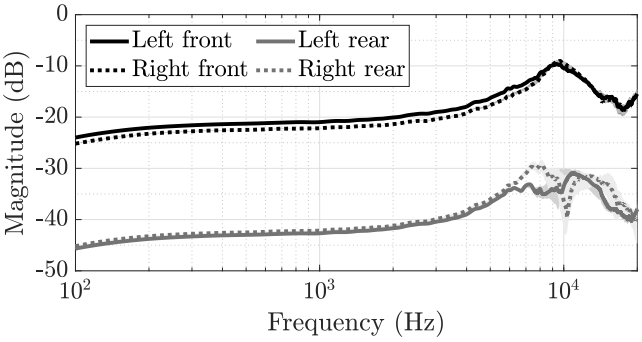

(a) Median free-field magnitude spectra with interquartile ranges of the front and rear research HA microphone pairs, evaluated for directions in the horizontal plane. Note that the curves for the rear microphone pair was shifted by −20 dB for increased readability.

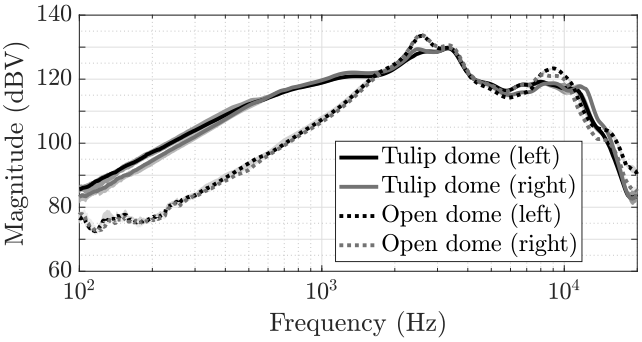

(b) Median SPL transfer functions of the research HA receivers with interquartile ranges and different ear pieces attached. (Figure taken from [41], licensed under CC BY 4.0, and adapted.)

Figure 9: Acoustic characterisation of the research HA microphones and receivers.

3.4.3 Hearing aid receiver characteristics

I measured the HA receiver transfer functions with two typically used open-fit silicone ear pieces attached, namely an open dome and a tulip dome. The research HAs with different ear pieces were sequentially inserted into the artificial head with ear simulator, see Section 3.2. IR measurements were conducted in MATLAB™ [11] using exponentially swept sines in a frequency range between 20 Hz and 20 kHz with a length of 2^{18} samples at a sampling frequency of 44.1 kHz. The calibrated hardware measurement chain consisted of an audio interface (RME Fireface UC, Audio AG, Haimhausen, Germany) in combination with a charge amplifier (Type 2690-A, Nexus, Brüel & Kjær, Nærum, Den-

Table 1: Loudspeakers used for the spatial audio reproduction setups in the different experimental environments. The loudspeaker numbers in the first column correspond to the sampling grid nodes of the 16-channel spherical-cap loudspeaker array in the VR laboratory, see Figure 12a.

		Experimental environment			
Nr.	Type	Commercial hearing booth	Custom-made hearing booth	MobiLab	VR laboratory
1	KH 120 AW			×	×
2	O 110				×
3	O 110				×
4	O 110				×
5	O 110				×
6	O 110 D	×			×
7	O 110 D				×
8	KH 120 AW			×	×
9	KH 120 AW			×	×
10	O 110 D				×
11	O 110 D	×			×
12	KH 120 A		×		×
13	KH 120 AW			×	×
14	KH 120 A		×		×
15	KH 120 A		×		×
16	KH 120 A		×		×
	O 110 D	×			
	O 110 D	×			

mark). To avoid excessive non-linearities, all measurements were performed at an output voltage of −20 dBV. Since some variation can be expected when inserting the silicone ear pieces, the measurements were repeated ten times, each time after re-inserting the respective ear piece. The median measurement results with interquartile ranges are plotted in Figure 9b. Typical energy peaks around 3 kHz and 9 kHz, representing the first and second resonance frequencies of the ear simulator, respectively, can be observed. Both HA receivers additionally show comparable SPL transfer functions per device, independent from the ear piece used. Due to reduced leakage and a more pronounced pressure chamber effect [62, 66], the tulip ear piece exhibit more energy in the low frequency range.

3.5 4-channel loudspeaker arrays

The commercial hearing booth, see Section 2.1, was equipped with four loudspeakers (O 110 D, Klein + Hummel, Ostfildern/Kemnat, Germany), cf. Table 1. The loudspeakers were installed at azimuth angles of $\varphi = \{40°, 140°, 220°, 320°\}$ and a distance of approximately 1.2 m, relative to the centre of the listener's interaural axis. A similar set of four loudspeakers was mounted in the custom-made hearing booth at azimuth angles of $\varphi = \{45°, 135°, 225°, 315°\}$ and a distance of about 1.1 m, see Table 1 and Figure 10. The vertical rods and mounts allow adjustment of the heights and yaw angles of the loudspeakers at fixed azimuth angles. Additional tilt-able clamping pieces can be used to adjust the pitch angles in a way that the main axes intersect with the centre of the listener's interaural axis to meet a recommended installation at elevated positions for less pronounced notches and azimuthal variations in the playback HRTFs using acoustic crosstalk cancellation systems [67].

3.6 16-channel spherical-cap loudspeaker array

Representing another option of an experimental environment, a reproduction setup with commercially available hardware was implemented. The setup was temporarily installed in the VR laboratory of the institute, see Section 2.3, and consisted of $N_{VR} = 16$ comparable active 2-way loudspeakers with front bass-reflex ports, see Table 1.

3.6.1 Loudspeaker transfer functions

To explore the effects of manufacturing tolerances and differences in acoustic properties between the loudspeaker models, installed in the different experimental environments, IR measurements were conducted in the hemi-anechoic chamber, see Section 2.4. These measurements were performed in two different sessions, each time with the loudspeaker placed on the floor 2 m away from and with its main axis tilted towards the measurement microphone (40 AF, G.R.A.S. Sound & Vibration A/S, Holte, Denmark; Type 2669, Brüel & Kjær, Nærum, Denmark), which was operated in combination with a measuring amplifier (Type 2610 or Type 2690-A, Nexus, Brüel & Kjær, Nærum, Denmark) and an audio interface (RME Hammerfall DSP Multi-

Figure 10: Custom-made hearing booth. (Photo taken from [17], licensed under CC BY 4.0, and adapted.)

face II, Audio AG, Haimhausen, Germany). As excitation signal, exponentially swept sines between 20 Hz and 20 kHz were generated in MATLAB™, exhibiting a length of 2^{18} samples at a sampling rate of 44.1 kHz. The obtained IRs were time-windowed using two one-sided Hann windows with a 3 ms fade-in after 0 ms and a 15 ms fade-out after 100 ms. For ease of comparison, all magnitude transfer functions were normalised to unity at 1 kHz, see Figure 11a. Due to the distinct room modes around 54 Hz and 75 Hz, the magnitude spectra below the lower frequency limit of 100 Hz, see Section 2.4, should be interpreted accordingly. Above 100 Hz, the relative loudspeaker magnitude transfer functions showed comparable curve progressions, fluctuating around an average value of −1.7 dB with minimum and maximum values of −6.3 dB and 2.6 dB, respectively. In view of the expected disproportionately large influence of the room acoustics in the VR laboratory and the already very flat frequency responses, no spectral EQ was applied.

3.6.2 Physical array implementation

The loudspeakers were subsequently arranged on an equal-area sampling grid [68] of order $\mathcal{N}_{\mathrm{VR}} = 3$ and a nominal array radius of $R_{\mathrm{VR}} = 1.7\,\mathrm{m}$, with removed south pole, see Figures 12a and 12b. All loudspeakers were positioned and oriented using two self-levelling cross-line lasers (GLL 3-80, Bosch Professional, Gerlingen-Schillerhöhe, Germany) and an electronic spirit level. The optical tracking system, see Section 3.1, was used to verify the loudspeaker positions. After calibrating the system with the wand (CW-500, NaturalPoint, Inc. DBA OptiTrack, Corvallis, OR, USA), the horizontal centre of the array, marked on the floor, was defined as the origin of the global coordinate system utilising the calibration square (CS-100, NaturalPoint, Inc. DBA OptiTrack, Corvallis, OR, USA). Subsequently, this centre was vertically translated to match the nominal array centre at a height of 1.35 m. I used a 70 cm long carbon fibre rod with an attached tetrahedral rigid body, consisting of four reflective markers, to measure the actual loudspeaker positions. After translating the pivot point of the rigid body to the tip of the rod, the actual loudspeaker positions, defined by the nominal centre of each loudspeaker between the low-/mid-frequency driver and the tweeter coinciding with the vertical loudspeaker axis, were measured through single-shot measurements [11]. The results of these measurements are shown in Figure 12a. Figure 12c displays the corresponding deviations from the ideal directions, divided into azimuth, zenith and overall angular error components, ε_R, ε_φ, ε_θ and ε_γ, respectively.

The results regarding the radial error component were obtained based on estimating the acoustic distance. For this purpose, I placed a measurement microphone (Type 4190 and 2669, Brüel & Kjær, Nærum, Denmark), operated with a microphone conditioning amplifier (Type 2690-A, Nexus, Brüel & Kjær, Nærum, Denmark) and an A/D converter (RME Octamic XTC and Madiface XT, Audio AG, Haimhausen, Germany), at the nominal array centre. The IR measurements were conducted using exponential sweeps of length 2^{17} samples. Figure 12c shows the actual radial error with respect to R_{VR} without the north pole loudspeaker, which was installed at a distance of 0.99 m due to spatial restrictions. After upsampling the IRs by a factor of eight, the temporal start instances of the IRs and the corresponding loudspeaker distances were estimated and subtracted from the nominal start instances, corresponding to the nominal array radius. The resulting time differences were subsequently used to shift the measured IRs in time at their original sampling rate. This resulted in average virtual radius deviations of approximately 0 ± 2 mm ($\mu \pm \sigma$, range: −3 mm to 3.5 mm). Note that the corresponding black error bars are not shown in Figure 12c due to the small error magnitudes.

The reproduction levels were adjusted by calculating and matching the RMS energy of the measured loudspeaker magnitude transfer functions to the one of the frontal centre loudspeaker, that is, loudspeaker 11, see Figure 12a. The spectral energy levels per individual loudspeaker were subsequently estimated by the RMS energy per third-octave band and compared to the mean RMS energy per third-octave band averaged across all loudspeakers. Figure 11b shows the results

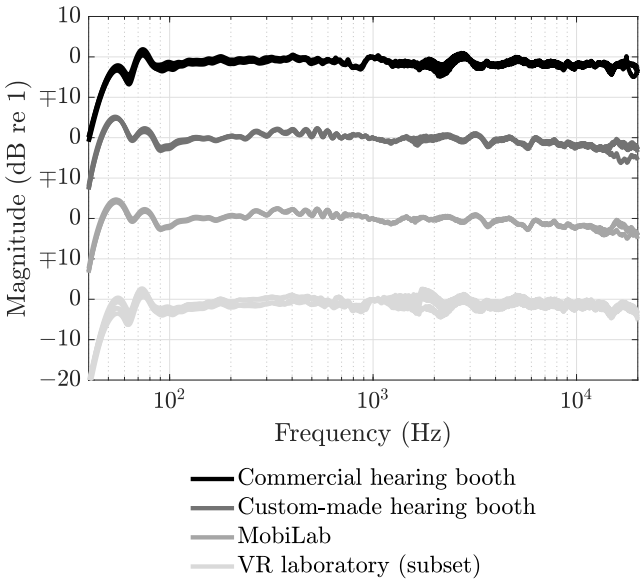

(a) Ideal on-axis magnitude frequency responses based on measurements conducted in the hemi-anechoic chamber. Results are normalised to unity at 1 kHz. For increased readability, the curves were shifted by 20 dB with respect to the previous one and grouped per experimental environment.

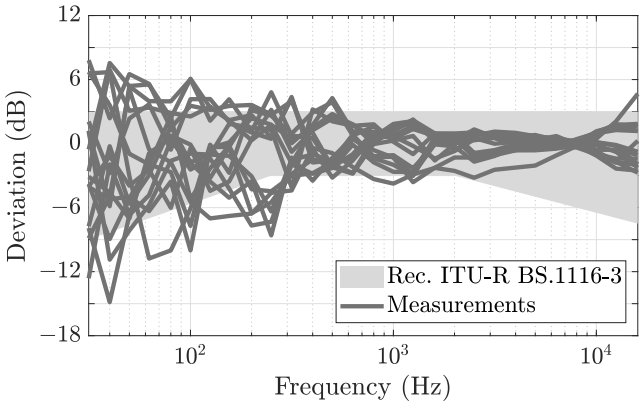

(b) Comparison of the tolerance range for room response curves, specified by ITU-R BS.1116-3 [20], with the RMS energy deviation per loudspeaker and third-octave band from the mean RMS energy per third-octave band, averaged across all loudspeakers included in the 16-channel loudspeaker array of the VR laboratory, measured in situ at the nominal sweet spot.

Figure 11: Acoustic characterisation of the loudspeakers installed in the different experimental environments, see Table 1.

together with the tolerance range for room response curves, specified in ITU-R BS.1116-3 [20]. Note that I used exponentially swept sines instead of pink noise as measurement signal and a modified level alignment criterion. While deviations in third-octave bands with centre frequencies above 400 Hz are largely within the recommended tolerance range, violations were mainly observed in the frequency bands below, which can be attributed to the placement of loudspeakers in the upper and lower rings very close to ceiling and floor, respectively, as well as the combination of too high RTs, see Figure 5a, and the influence of room modes. The overruns and underruns ranged from 8 dB to −15 dB, respectively.

3.7 68-channel spherical-cap loudspeaker array

A spherical-cap loudspeaker array with $N_{AC} = 68$ loudspeakers for spatial audio reproduction using various reproduction methods was installed in the anechoic chamber, see Section 2.5. The array design and implementation are presented in depth by Pausch, Behler, and Fels [37].

3.8 Measurement arm

Figure 13 shows a setup for measuring generic receiver directivities of an example artificial head with ear simulator, see Section 3.2, in a step-wise measurement procedure. In this setup, installed in the hemi-anechoic chamber, see Section 2.4, the artificial head is placed on a remote-controlled turntable with stepping motor for an azimuthal rotation with a pre-defined step size. A custom-made broadband loudspeaker with front bass-reflex ports, equipped with a 2″ driver (OmnesAudio BB2.01, Blue Planet Acoustic, Frankfurt, Germany) and a frequency range of 200 Hz–20 kHz [64], is attached to a 3-point traverse that can be positioned via another remote-controlled stepping motor to sample a line of longitude of the measurement sphere at a pre-defined spatial resolution between zenith angles of $0° \leq \theta \leq 120°$ and a radius of 1.86 m. If directions below the maximum zenith angle are also to be measured, it is necessary to mount the artificial head upside down, to subsequently merge the results from the upper and lower hemispheres [41, 64]. This makes it possible to obtain reference spatial transfer functions on arbitrary spatial grids [11, 31, 32, 69].

3.9 Measurement arc

Also installed in the hemi-anechoic chamber, see Section 2.4, and designed as a system to measure individual receiver directivities [32], 64 1-inch full-range loudspeakers (W1-2025SA, Tang Band, Taipei, Taiwan) were built into identically designed closed 0.05 l arc segments, resulting in an effective frequency range of about 500 Hz to 18 kHz. As shown in Figure 14, the arc segments form an arc-shaped line array, representing a line of longitude of the measurement sphere, and cover zenith angles of $1.25° \leq \theta \leq 160°$, arranged in increments of 2.52 deg. A measurement radius of 1.2 m allows to capture HRTF characteristics that are relevant for auditory localisation in the distal region, that is, beyond an egocentric distance of 1 m [70]. Using a remote-controlled stepping motor, the array can be rotated around the vertical axis, ideally coinciding with the longitudinal axis running through the centre of the interaural axis, at a pre-defined speed for continuous HRTF measurements [71, 72]. This concept allows to measure directional transfer functions on an equian-

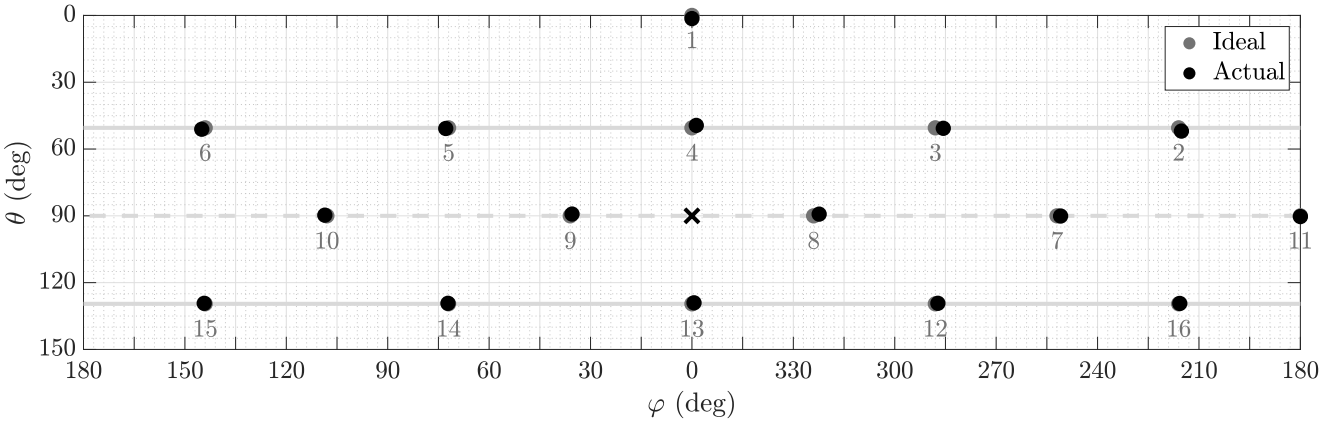

(a) Ideal and actual sampling layouts, represented by grey and black dots, respectively, with loudspeaker channel numbers. The solid and dashed horizontal lines in light grey show the loudspeaker rings and the horizontal plane at the listener's nominal ear height, respectively, with the black cross indicating the default viewing direction.

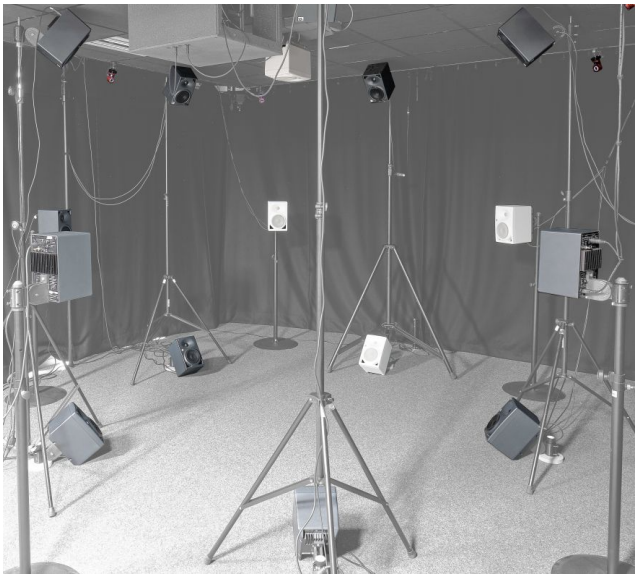

(b) Physical array implementation in the VR laboratory of the institute. (Photo licensed under CC BY-SA 4.0.)

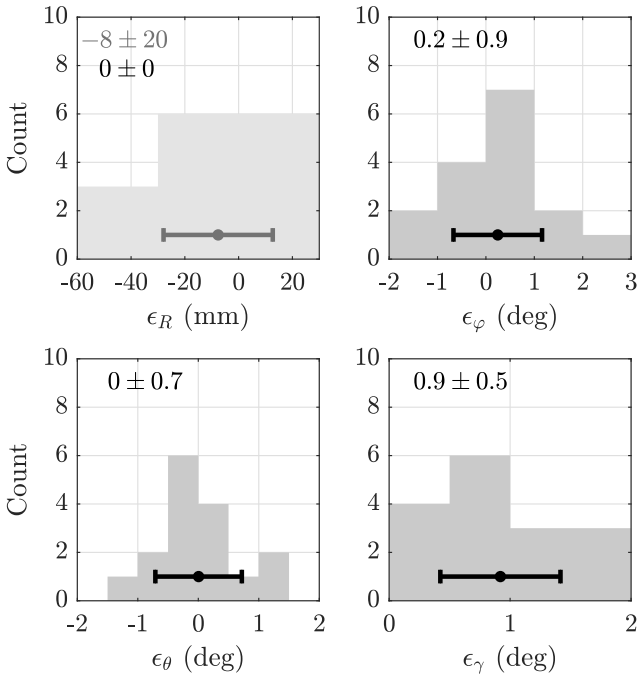

(c) Actual loudspeaker position errors. Histograms show the radial error ε_R, without the north pole loudspeaker and delayed loudspeaker signals (light grey), and azimuth, zenith and great circle central angle errors, ε_φ, ε_θ and ε_γ, respectively. Values in light grey and black correspond to μ and σ before and after delaying the loudspeaker signals, respectively, the former scenario also represented by the grey error bar, respectively.

Figure 12: 16-channel spherical-cap loudspeaker array.

gular spatial sampling with fixed and variable resolutions in elevation and azimuth angles, respectively [50, 73]. For further details on the array, its implementation and evaluation, the reader is referred to [32, 72, 74].

4 Conclusion

This report documented the experimental environments and hardware for spatial measurements and audio reproduction used in the experiments presented by Pausch [1], including measurement-based acoustic evaluations. It was shown how to construct a financially favourable but acoustically effective hearing booth whose room acoustic properties allow for sufficient in-situ channel separation for loudspeaker-based binaural reproduction [1, 31, 75]. The efforts undertaken to optimise the room acoustics of the VR laboratory were not sufficient to meet the demands of ITU-R BS.1116-3 [20] in terms of recommended relative RTs, requiring further measures, particularly in the low fre-

Figure 13: Measurement system for the acquisition of generic receiver directivities on a pre-defined spatial measurement grid, showing an artificial head equipped with an ear simulator as per ITU-T P.57 [25] and attached to a turntable for azimuthal rotation. The measurement loudspeaker is mounted on an arm to sample a line of longitude of the measurement sphere. (Photo licensed under CC BY-SA 4.0.)

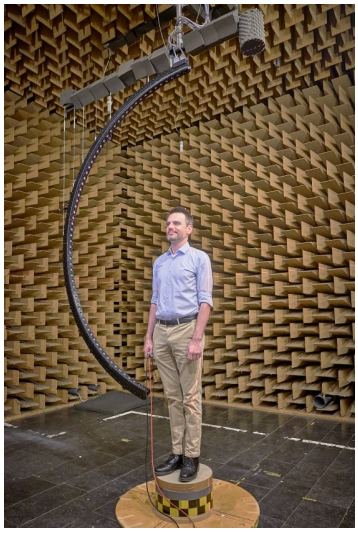

Figure 14: Measurement system for the acquisition of individual receiver directivities, showing a participant equipped with two in-ear microphones. The arc-shaped loudspeaker array is rotated around the participant for continuous HRTF measurements. (Photo licensed under CC BY 4.0.)

quency range. While there were distinct high-frequency differences between the rear HA microphone magnitude transfer functions of the research HAs, the measurement results of the front HA microphone pair and the HA receivers were comparable. In combination with the analysis of the ear piece-dependent passive damping properties, these investigations are helpful for complementary analysis of perceptual results in combined reproduction [7]. Different implementations of loudspeaker arrays with increasing complexity were presented. These reproduction setups were successfully applied in experiments involving children and adults with normal hearing, and children with hearing loss, fitted with the aforementioned research HAs [1, 7, 16, 17, 76]. Together with the two systems to measure generic and individual receiver directivities at a high spatial resolution, it was possible to accommodate the wide range of measurement tasks and specific requirements for the development of the results in [1].

List of acronyms

A/D	analog-to-digital
ANL	ambient noise level
D/A	digital-to-analog
EQ	equalisation
HA	hearing aid
HRTF	head-related transfer function
IR	impulse response
MobiLab	mobile laboratory
MPANL	maximum permissible ambient noise level
RMS	root mean square
RT	reverberation time
SPL	sound pressure level
VR	virtual reality

Acknowledgments

The author appreciates the valuable assistance from the team of the mechanical workshop, Uwe Schlömer, Thomas Schaefer and Mark Eiker, as well as by Rolf Kaldenbach, Gottfried Behler, Martin Guski, Jonas Stienen, Michael Kohnen, Johannes Klein, Marco Berzborn, Mark Müller-Giebeler, Ingo Witew and Lukas Aspöck. Special thanks go to the ITA-Toolbox development team. Judith Verberne, Matthew McKee and Todd Fortune from GN ReSound and Per Blysa from Sonion kindly provided the research HA prototypes and cables.

Declaration of conflicting interests

The author declared no conflicts of interest with respect to the research, authorship, and/or publication of this report. GN ReSound and Sonion only provided the hardware and were not involved in any other stage. The author had full access to all of the data in this report and takes complete responsibility for the integrity of the data and the accuracy of the data analysis.

Funding

The large part of this work was supported by the European Union's Seventh Framework Programme for research, technological development and demonstration (ITN FP7-607139, Improving Children's Auditory Rehabilitation).

ORCID iD

Florian Pausch https://orcid.org/0000-0003-2728-3170

References

[1] F. Pausch, "Spatial audio reproduction for hearing aid research: System design, evaluation and application," Dissertation, RWTH Aachen University, Aachen, Germany, 2022. DOI: 10.18154/RWTH-2022-03745.

[2] R. A. Viveros Munoz, "Speech perception in complex acoustic environments: Evaluating moving maskers using virtual acoustics," Dissertation, RWTH Aachen University, Aachen, Germany, 2019. DOI: 10.18154/RWTH-2019-07497.

[3] ISO 8253-1, "Acoustics – Audiometric test methods – Part 1: Pure-tone air and bone conduction audiometry," International Organization for Standardization, Geneva, Switzerland, Norm ISO 8253-1:2010, 2010.

[4] ISO 8253-2, "Acoustics – Audiometric test methods – Part 2: Sound field audiometry with pure-tone and narrow-band test signals," International Organization

for Standardization, Geneva, Switzerland, Norm ISO 8253-2:2009, 2009.

[5] ISO 8253-3, "Acoustics – Audiometric test methods – Part 3: Speech audiometry (ISO 8253-3:2012)," International Organization for Standardization, Geneva, Switzerland, Norm ISO 8253-3:2012, 2012.

[6] J. Oberem, "Examining auditory selective attention: From dichotic towards realistic environments," Dissertation, RWTH Aachen University, Aachen, Germany, 2020. DOI: 10.18154/RWTH-2020-04889.

[7] F. Pausch and J. Fels, "Localization Performance in a Binaural Real-Time Auralization System Extended to Research Hearing Aids," *Trends in Hearing*, vol. 24, pp. 1–18, 2020, PMID: 32324491. DOI: 10.1177/2331216520908704.

[8] A. Sæbø, "Influence of reflections on crosstalk cancelled playback of binaural sound," Dissertation, Faculty of Information Technology, Electrical Engineering, Norwegian University of Science, and Technology, Norway, 2001.

[9] M. Kohnen, J. Stienen, L. Aspöck, and M. Vorländer, "Performance Evaluation of a Dynamic Crosstalk-Cancellation System with Compensation of Early Reflections," in *Audio Engineering Society Conference: 2016 AES International Conference on Sound Field Control*, Audio Engineering Society, Guildford, UK, 2016, pp. 1–8.

[10] ISO 3382-2, "Acoustics – Measurement of room acoustic parameters - Part 2: Reverberation time in ordinary rooms," International Organization for Standardization, Geneva, Switzerland, Norm ISO 3382-2:2008-06, 2008.

[11] M. Berzborn, R. Bomhardt, J. Klein, J.-G. Richter, and M. Vorländer, "The ITA-Toolbox: An Open Source MATLAB Toolbox for Acoustic Measurements and Signal Processing," in *43th Annual German Congress on Acoustics, Kiel (Germany), 6 Mar 2017 - 9 Mar 2017*, Mar. 6, 2017, pp. 222–225.

[12] G. Behler, "An active loudspeaker point source for the measurement of high quality wide band room impulse responses," in *Proceedings of the Institute of Acoustics - Auditorium Acoustics 2018, Hamburg, Germany*, vol. 40, Hamburg, Germany: Institute of Acoustics, 2018, pp. 435–446.

[13] H. Kuttruff, *Room Acoustics*. CRC Press, 2016.

[14] L. G. Marshall, "An acoustics measurement program for evaluating auditoriums based on the early/late sound energy ratio," *The Journal of the Acoustical Society of America*, vol. 96, no. 4, pp. 2251–2261, 1994. DOI: 10.1121/1.410097.

[15] F. Pausch and J. Fels, "MobiLab – A Mobile Laboratory for On-Site Listening Experiments in Virtual Acoustic Environments," *Acta Acustica united with Acustica*, vol. 105, no. 5, pp. 875–887, 2019. DOI: doi:10.3813/AAA.919367.

[16] F. Pausch, Z. E. Peng, L. Aspöck, and J. Fels, "Speech perception by children in a real-time virtual acoustic environment with simulated hearing aids and room acoustics," in *22nd International Congress on Acoustics: ICA 2016*, Invited paper., Buenos Aires, Catholic University of Argentina: Asociacion de Acusticos Argentinos, Sep. 5, 2016.

[17] L. Bell, Z. E. Peng, F. Pausch, V. Reindl, C. Neuschaefer-Rube, J. Fels, and K. Konrad, "fNIRS Assessment of Speech Comprehension in Children with Normal Hearing and Children with Hearing Aids in Virtual Acoustic Environments: Pilot Data and Practical Recommendations," *Children*, vol. 7, no. 11, 2020. DOI: 10.3390/children7110219.

[18] A. Lundeby, T. E. Vigran, H. Bietz, and M. Vorländer, "Uncertainties of Measurements in Room Acoustics," *Acta Acustica united with Acustica*, vol. 81, no. 4, pp. 344–355, 1995.

[19] L. Aspöck, F. Pausch, J. Stienen, M. Berzborn, M. Kohnen, J. Fels, and M. Vorländer, "Application of virtual acoustic environments in the scope of auditory research," *Proceedings of XXVIII Encontro da Sociedade Brasileira de Acústica*, 2018.

[20] ITU-R BS.1116-3, "Methods for the subjective assessment of small impairments in audio systems," International Telecommunication Union: Radiocommunication, Geneva, Switzerland, Recommendation, Feb. 2015.

[21] U. Ingard, "On the Theory and Design of Acoustic Resonators," *The Journal of the Acoustical Society of America*, vol. 25, no. 6, pp. 1037–1061, 1953. DOI: 10.1121/1.1907235.

[22] J.-F. Allard and Y. Champoux, "New empirical equations for sound propagation in rigid frame fibrous materials," *The Journal of the Acoustical Society of America*, vol. 91, no. 6, pp. 3346–3353, 1992. DOI: 10.1121/1.402824.

[23] S. Pelzer, M. Aretz, and M. Vorländer, "Quality assessment of room acoustic simulation tools by comparing binaural measurements and simulations in an optimized test scenario," in *Proc. Forum Acusticum Aalborg*, 2011.

[24] ISO 354:2003, "Acoustics – Measurement of sound absorption in a reverberation room," International Organization for Standardization, Geneva, Switzerland, Norm ISO 354:2003), 2003.

[25] ITU-T P.57, "Series P: Terminals and subjective and objective assessment methods - Objective measuring apparatus: Artificial ears," International Telecommunication Union, Geneva, Switzerland, Recommendation ITU-T P.57 (04/2009), 2009.

[26] ISO/R 1996:1971, "Acoustics – Description, measurement and assessment of environmental noise – Part 1: Basic quantities and assessment procedures," International Organization for Standardization, Geneva, Switzerland, Norm ISO/R 1996:1971, 1971, Withdrawn.

[27] M. Guski, "Influences of external error sources on measurements of room acoustic parameters," Dissertation, Institute of Technical Acoustics, RWTH Aachen University, Germany, Aachen, 2015.

[28] L. Aspöck, F. Brinkmann, D. Ackermann, S. Weinzierl, and M. Vorländer, "BRAS - Benchmark for Room Acoustical Simulation," Technical Report, 2020. DOI: 10.14279/depositonce-6726.3.

[29] L. L. Beranek and H. P. Sleeper, "The Design and Construction of Anechoic Sound Chambers," *The Journal of the Acoustical Society of America*, vol. 18, no. 1, pp. 140–150, 1946. DOI: 10.1121/1.1916351.

[30] DIN EN IEC 60268-21, "Sound system equipment – Part 21: Acoustical (output-based) measurements (IEC 6026821:2018); German version EN IEC 6026821:2018," German Institute for Standardization, e.V., Berlin, Germany, Norm DIN EN IEC 60268-21, Nov. 2019.

[31] B. Sanches Masiero, "Individualized Binaural Technology: Measurement, Equalization and Perceptual Evaluation," Dissertation, RWTH Aachen University, Aachen, Germany, 2012.

[32] J.-G. Richter, "Fast measurement of individual head-related transfer functions," Dissertation, RWTH Aachen University, Aachen, Germany, 2019. DOI: 10.18154/RWTH-2019-04006.

[33] F. Pausch, S. Doma, and J. Fels, "Hybrid multiharmonic interaural time difference model for individual behind-the-ear hearing aid-related transfer functions," *Institute for Hearing Technology and Acoustics, RWTH Aachen University*, 2021, Unpublished manuscript, in review.

[34] B. Philippen, "Transfer path analysis based on in-situ measurements for automotive applications," Dissertation, RWTH Aachen University, Aachen, Germany, 2017.

[35] M. Jaeger, P. Drichel, M. B. Müller-Giebeler, M. Schröder, J. K. Berroth, G. K. Behler, K. Hameyer, G. Jacobs, and M. Vorländer, "Erweiterung der Simulationsmöglichkeiten für maschinenakustische Untersuchungen an E-Motive-Antrieben im Kontext zur Fahrzeugstruktur," Tech. Rep. FVA-Forschungsbericht Heft Nr. 1370 "Erweiterung NVH Simulationsmodell" FVA 682 II, 2019.

[36] ISO 3744:2010, "Acoustics – Determination of sound power levels and sound energy levels of noise sources using sound pressure - Engineering methods for an essentially free field over a reflecting plane," International Organization for Standardization, Geneva, Switzerland, Standard, 2010.

[37] F. Pausch, G. Behler, and J. Fels, "SCaLAr – A surrounding spherical cap loudspeaker array for flexible generation and evaluation of virtual acoustic environments," *Acta Acust.*, vol. 4, no. 5, p. 19, 2020. DOI: 10.1051/aacus/2020014.

[38] A. W. Mills, "On the Minimum Audible Angle," *The Journal of the Acoustical Society of America*, vol. 30, no. 4, pp. 237–246, 1958. DOI: 10.1121/1.1909553.

[39] J. Blauert, *Spatial Hearing: The Psychophysics of Human Sound Localization*. Cambridge, Mass. MIT Press, 1997.

[40] T. Okano, "Judgments of noticeable differences in sound fields of concert halls caused by intensity variations in early reflections," *The Journal of the Acoustical Society of America*, vol. 111, no. 1, pp. 217–229, 2002. DOI: 10.1121/1.1426374.

[41] F. Pausch, L. Aspöck, M. Vorländer, and J. Fels, "An Extended Binaural Real-Time Auralization System With an Interface to Research Hearing Aids for Experiments on Subjects With Hearing Loss," *Trends in Hearing*, vol. 22, pp. 1–32, 2018. DOI: 10.1177/2331216518800871.

[42] J. Oberem, V. Lawo, I. Koch, and J. Fels, "Intentional Switching in Auditory Selective Attention: Exploring Different Binaural Reproduction Methods in an Anechoic Chamber," *Acta Acustica united with Acustica*, vol. 100, no. 6, pp. 1139–1148, 2014. DOI: doi:10.3813/AAA.918793.

[43] Polhemus, *Motion Tracking Technical Comparisons - Tracking Performance*, https://polhemus.com/_assets/img/Polhemus_Tracking_Performance_Comparison_Chart.pdf, https://polhemus.com/_assets/img/Polhemus_Tracking_Performance_Comparison_Chart.pdf, accessed on 2021-04-29, Sep. 2018.

[44] NaturalPoint Inc., *Flex 13*, https://optitrack.com/products/flex-13/, https://optitrack.com/products/flex-13/, accessed on 2021-04-29, 2021.

[45] F. Pausch, M. Kohnen, L. Aspöck, Z. E. Peng, and J. Fels, "Investigation of sound localization performance in a virtual acoustic environment designed for hearing aid users," in *42th German Annual Conference on Acoustics: DAGA 2016, Aachen, 14-17 March*, Mar. 17, 2016, pp. 1124–1127.

[46] VIRTUAL ACOUSTICS, *A real-time auralization framework for scientific research, Institute of Technical Acoustics, RWTH Aachen University*, Available at http://www.virtualacoustics.org/, accessed on 2022-01-18, 2021.

[47] J. Stienen, "Real-time Auralisation of Outdoor Sound Propagation," Dissertation, RWTH Aachen University, Aachen, Germany, 2022.

[48] J. Fels and M. Vorländer, "Anthropometric Parameters Influencing Head-Related Transfer Functions," *Acta Acustica united with Acustica*, vol. 95, no. 2, pp. 331–342, 2009. DOI: 10.3813/AAA.918156.

[49] M. Vorländer, *Auralization - Fundamentals of Acoustics, Modelling, Simulation, Algorithms and Acoustic Virtual Reality*. Springer, 2020.

[50] H. S. Braren and J. Fels, "Towards Child-Appropriate Virtual Acoustic Environments: A Database of High-Resolution HRTF Measurements and 3D-Scans of Children," *International Journal of Environmental Research and Public Health*, vol. 19, no. 1, 2022. DOI: 10.3390/ijerph19010324.

[51] A. Schmitz, "Ein neues digitales Kunstkopfmeßsystem," *Acta Acustica united with Acustica*, vol. 81, no. 4, pp. 416–420, 1995.

[52] P. Minnaar, "Simulating an acoustical environment with binaural technology: Investigations of binaural recording and synthesis," *Acustica United with Acta Acustica*, vol. 88, no. 3, May/June, p. 286, 2002.

[53] H. Kayser, S. D. Ewert, J. Anemüller, T. Rohdenburg, V. Hohmann, and B. Kollmeier, "Database of Multichannel In-ear and Behind-the-ear Head-related and Binaural Room Impulse Responses," *EURASIP J. Adv. Signal Process*, vol. 2009, 6:1–6:10, Jan. 2009. DOI: 10.1155/2009/298605.

[54] C. Oreinos and J. M. Buchholz, "Measurement of a Full 3D Set of HRTFs for In-Ear and Hearing Aid Microphones on a Head and Torso Simulator (HATS)," *Acta Acustica united with Acustica*, vol. 99, no. 5, pp. 836–844, 2013. DOI: doi:10.3813/AAA.918662.

[55] F. Denk, S. M. A. Ernst, S. D. Ewert, and B. Kollmeier, "Adapting Hearing Devices to the Individual Ear Acoustics: Database and Target Response Correction Functions for Various Device Styles," *Trends in Hearing*, vol. 22, p. 2 331 216 518 779 313, 2018, PMID: 29877161. DOI: 10.1177/2331216518779313.

[56] R. Bomhardt, "Anthropometric individualization of head-related transfer functions analysis and modeling," Dissertation, Teaching and Research Area of Medical Acoustics, RWTH Aachen University, Aachen, Germany, 2017.

[57] F. Brinkmann, L. Aspöck, D. Ackermann, S. Lepa, M. Vorländer, and S. Weinzierl, "A round robin on room acoustical simulation and auralization," *The Journal of the Acoustical Society of America*, vol. 145, no. 4, pp. 2746–2760, 2019. DOI: 10.1121/1.5096178.

[58] S. Gilman and D. D. Dirks, "Acoustics of ear canal measurement of eardrum SPL in simulators," *The Journal of the Acoustical Society of America*, vol. 80, no. 3, pp. 783–793, 1986. DOI: 10.1121/1.393953.

[59] R. Schlieper, S. Li, S. Preihs, and J. Peissig, "Estimation of the Headphone "Openness" Based on Measurements of Pressure Division Ratio, Headphone Selection Criterion, and Acoustic Impedance," in *Audio Engineering Society Convention 145*, Oct. 2018.

[60] B. Masiero and J. Fels, "Perceptually Robust Headphone Equalization for Binaural Reproduction," in *Audio Engineering Society Convention 130*, London, UK: Audio Engineering Society, May 2011, pp. 1–7.

[61] A. Farina, "Advancements in Impulse Response Measurements by Sine Sweeps," in *Audio Engineering Society Convention 122*, May 2007.

[62] C. Poldy, "Headphones," in *Loudspeaker and Headphone Handbook*, Routledge, 2012, pp. 599–706.

[63] R. W. Sweetow and C. Z. Pirzanski, "The Occlusion Effect and Ampclusion Effect," in *Seminars in Hearing*, Thieme Medical Publishers, Inc., 333 Seventh Avenue, New York, NY 10001, USA, vol. 24, 2003, pp. 333–344.

[64] H. S. Braren and J. Fels, "A High-Resolution Head-Related Transfer Function Data Set and 3D-Scan of KEMAR," Institute for Hearing Technology and Acoustics, RWTH Aachen University, Technical report, 2020. DOI: 10.18154/RWTH-2020-11307.

[65] O. Kirkeby, P. A. Nelson, H. Hamada, and F. Orduna-Bustamante, "Fast deconvolution of multichannel systems using regularization," *IEEE Transactions on Speech and Audio Processing*, vol. 6, no. 2, pp. 189–194, 1998.

[66] H. Dillon, *Hearing Aids*, 2nd edition. Boomerang Press; Thieme Sydney: New York, 2012.

[67] Y. L. Parodi and P. Rubak, "Objective evaluation of the sweet spot size in spatial sound reproduction using elevated loudspeakers," *The Journal of the Acoustical Society of America*, vol. 128, no. 3, pp. 1045–1055, 2010. DOI: 10.1121/1.3467763.

[68] P. Leopardi, "A partition of the unit sphere into regions of equal area and small diameter," *Electronic Transactions on Numerical Analysis*, vol. 25, no. 12, pp. 309–327, 2006.

[69] F. Zotter, "Sampling Strategies for Acoustic Holography/Holophony on the Sphere," in *NAG/DAGA 2009 International Conference on Acoustics, Rotterdam*, Mar. 2009, pp. 1107–1110.

[70] D. S. Brungart and W. M. Rabinowitz, "Auditory localization of nearby sources. Head-related transfer functions," *The Journal of the Acoustical Society of America*, vol. 106, no. 3, pp. 1465–1479, 1999. DOI: 10.1121/1.427180.

[71] J. He, R. Ranjan, and W. Gan, "Fast continuous HRTF acquisition with unconstrained movements of human subjects," in *2016 IEEE International Conference on Acoustics, Speech and Signal Processing (ICASSP)*, 2016, pp. 321–325.

[72] J.-G. Richter and J. Fels, "On the Influence of Continuous Subject Rotation During High-Resolution Head-Related Transfer Function Measurements," *IEEE/ACM Transactions on Audio, Speech, and Language Processing*, vol. 27, no. 4, pp. 730–741, 2019.

[73] R. Bomhardt, M. de la Fuente Klein, and J. Fels, "A high-resolution head-related transfer function and three-dimensional ear model database," *Proceedings of Meetings on Acoustics*, vol. 29, no. 1, p. 050 002, 2016. DOI: 10.1121/2.0000467.

[74] J.-G. Richter and J. Fels, "Evaluation of Localization Accuracy of Static Sources Using HRTFs from a Fast Measurement System," *Acta Acustica united with Acustica*, vol. 102, no. 4, pp. 763–771, 2016. DOI: 10.3813/AAA.918992.

[75] Y. L. Parodi and P. Rubak, "A Subjective Evaluation of the Minimum Channel Separation for Reproducing Binaural Signals over Loudspeakers," *Journal of the Audio Engineering Society*, vol. 59, no. 7/8, pp. 487–497, 2011.

[76] Z. E. Peng, F. Pausch, and J. Fels, "Spatial release from masking in reverberation for school-age children," *The Journal of the Acoustical Society of America*, vol. 150, no. 5, pp. 3263–3274, 2021. DOI: 10.1121/10.0006752.